We are IntechOpen, the world's leading publisher of Open Access books Built by scientists, for scientists

6,900
Open access books available

185,000
International authors and editors

200M
Downloads

Our authors are among the

154
Countries delivered to

TOP 1%
most cited scientists

12.2%
Contributors from top 500 universities



WEB OF SCIENCE™

Selection of our books indexed in the Book Citation Index in Web of Science™ Core Collection (BKCI)

Interested in publishing with us?
Contact book.department@intechopen.com

Numbers displayed above are based on latest data collected.
For more information visit www.intechopen.com



Chapter 1

Fatigue Failure Analysis of a Centrifugal Pump Shaft

Mohd Nasir Tamin and Mohammad Arif Hamzah

Additional information is available at the end of the chapter

http://dx.doi.org/10.5772/intechopen.70672

Abstract

This chapter deliberates on the systematic processes in failure investigation of engineering components and structures. The procedures are demonstrated in performing failure analysis of a centrifugal pump shaft. The chemical, microstructural, and fractographic analyses provide information on the material science aspects of the failure. The mechanical design analyses establish the cause of failure based on the stress calculations using the strength-of-materials approach. Fatigue analysis using the modified Goodman criterion is employed with consideration of yielding, under the fluctuating load. It is concluded that fatigue crack nucleated in the localized plastic zone at the threaded root region and propagated to cause the premature fatigue failure of the rotor shaft.

Keywords: high-cycle fatigue, mean stress effect, modified Goodman criterion, rotor shaft, stress analysis

1. Introduction

Pumps are commonly used to transport fluids such as water, sewage, petroleum, and petrochemical products. The pumps can be divided into two general categories, namely dynamic pumps and displacement pumps. In a dynamic pump, such as a centrifugal pump, energy is added to the pumping medium continuously and the medium is not contained in a set volume. The energy, in a displacement pump such as a diaphragm pump, is added to the pumping medium periodically while the medium is contained in a set volume. The pump is driven by a prime mover that is either an engine or an electric motor. The capacity of a pump is defined based on the pressure head (in meters) and the maximum delivery flow rate at a specific speed of the shaft. The latter is related to the required power of the prime mover. Typical specifications of some pumps are shown in **Table 1**.

The main components of a centrifugal pump are the rotor assembly and the casing. The pump rotor assembly comprises the shaft, impeller, sleeves, seals, bearings, and coupling halves, as

INTECH
open science | open minds

© 2017 The Author(s). Licensee InTech. This chapter is distributed under the terms of the Creative Commons Attribution License (http://creativecommons.org/licenses/by/3.0), which permits unrestricted use, distribution, and reproduction in any medium, provided the original work is properly cited. CC BY

Parameter	*Pump A*	*Pump B*	*Pump C*	*Pump D*
Suction head (m)	33	24	30	32
Delivery volume (m^3/h)	32	120	150	9
Motor power (kW)	7.5	15	37	2.2
Speed (rpm)	2900	1450	1450	2900

Table 1. Typical specifications of centrifugal pump systems for various applications.

illustrated in **Figure 1**. The spiral-shaped casing or volute surrounding the pump impeller serves to collect the fluid discharged by the impeller. The impeller is a rotating set of vanes designed to impart rotation to the mass of the pumping medium. The coupling halves connect the rotor shaft to the output shaft of the motor.

During operation, the engine or the electric motor drives the pump rotor assembly. The rotational kinetic energy is converted to the hydrodynamic energy of the fluid flow. The fluid enters the pump axially through the eye of the casing and is caught in the impeller blades. The fluid gains both velocity and pressure while being accelerated by the impeller. It is then whirled tangentially and radially outward until it leaves through all circumferential parts of the impeller into the diffuser part of the casing. The doughnut-shaped diffuser or scroll section of the casing decelerates the flow and further increases the pressure.

The shaft of the rotor experiences both cyclic flexural load and torsional load during the pumping operation. The start-and-stop cycles could also induce fluctuating stresses with high mean stress level. In this respect, often, the classical high-cycle fatigue analysis is considered in

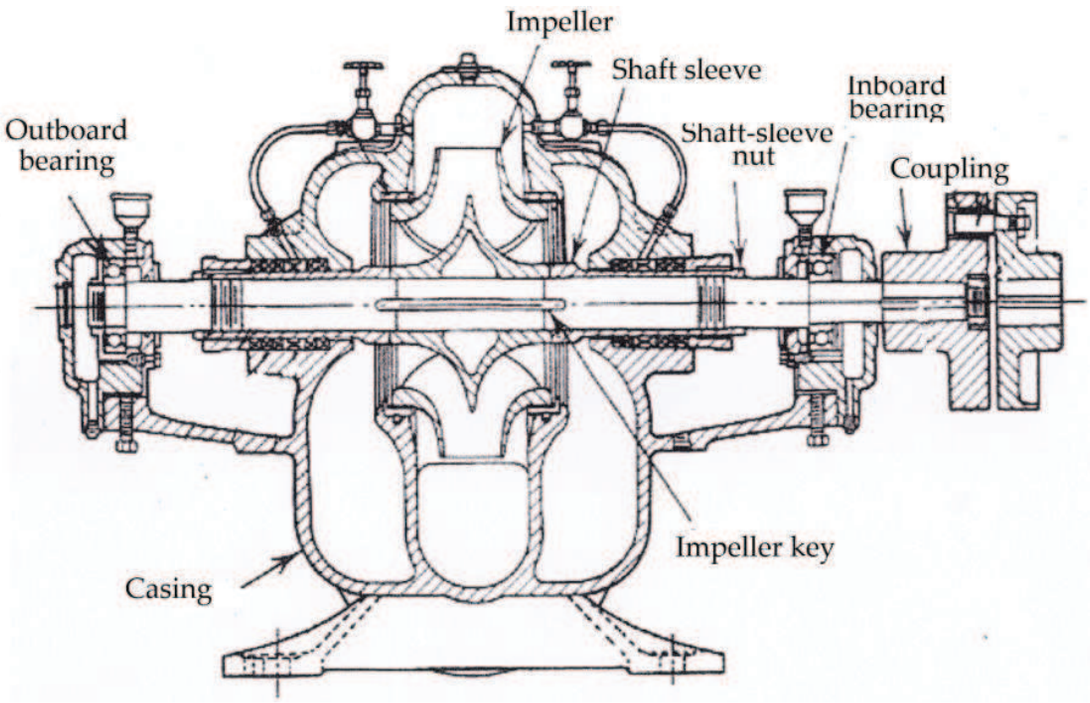


Figure 1. Cut-out section of a centrifugal pump, illustrating the main components.

the safe design of the shaft. The stress analysis on the shaft accounts for the stress raisers due to various design features including fillet, groove, keyway, and screw threads. The presence of such design features, combined with the complex loading, calls for the computational assessment on the reliability of the shaft employing the finite element analysis. In addition, the design should also consider the rotor dynamics aspect (critical speed) of the shaft.

2. Failure and the failure analysis

Experience indicates that despite adhering to the available design procedures, premature failure of the rotor shaft during operation of the centrifugal pump is still reported. The causes of such failure could be classified based on (a) faulty design or misapplication of the materials, (b) faulty processing or fabrication, and (c) the deterioration in service of the component. The severe localized stress due to the design features, as mentioned earlier, could induce excessive plastic deformation leading to the nucleation of fatigue cracks. Fatigue cracks could also nucleate from inherent defects in the material such as nonmetallic inclusions and microvoids, and from machining-induced surface irregularities. In-service deterioration is manifested in the wear of the material, in the form of galling and stress corrosion cracking. The applied fatigue loading continuously causes degradation of the modulus and strength properties of the material. Additional factors that may contribute to early failure of the shaft include poor maintenance of the pump assembly, and improper service and repair of the component.

Procedures	Description	For centrifugal rotor shaft
Description of the failure situation	Background information and service history, records on abnormal operation.	Frequency of start-and-stop operations, details of repair works done, component life.
Visual inspection	Examine the failed component for obvious failure features.	Location of fracture along the shaft, beach lines as sign of fatigue failure.
Mechanical design analysis	Determine if the part is of sufficient size and reliability/life.	Fatigue analysis to demonstrate "infinite life" of the shaft.
Chemical design analysis	Establish the suitability of the material with respect to corrosion resistance.	Determine the chemical composition of the shaft material.
Metallographic examination	To help establish such facts as whether the part has correct heat treatment.	Identify heat treatment of the shaft through the analysis of microstructure and hardness measures.
Determine properties	Determine the properties of the material, pertinent to the design.	Refer to the material data sheets for the grade of the alloy.
Failure simulation	Establish the response of the component under identical loading and boundary conditions.	Finite element simulation of the shaft to establish the stress field in the failed region.
Report writing	Written report detailing the results of the analysis and the causes of failure. May include recommendations to prevent the occurrence of similar failure situation.	To deliberate the rationale on the causes of the premature failure of the shaft.

Table 2. Steps in performing failure analysis of engineering components and structures.

Once the undesirable failure event occurred, assessment on the extent of damage to the component and its impact to the overall integrity of the system is required. Failure analysis on the failed component is performed to determine the root causes of the failure, thus appropriate steps could be implemented to prevent similar occurrence in the future. The process flow of the failure analysis is summarized in **Table 2**.

This chapter describes the procedures and steps in performing failure analysis. A case study on the failure of the rotor shaft of a centrifugal pump is used for illustration. Adequate discussion on the relevant aspects of the analysis in each step is provided. The methodology presented in this chapter could easily be employed and/or extended in performing failure analysis of engineering components and structures.

3. Description of the failure situation

It was reported that the shaft of a centrifugal pump used to pump the blending of hydrocarbons to deliver the final oil product in a refinery has failed during operation. The failure resulted in a fire of the pump and the piping works of the refinery within the unit, with an estimated total loss of USD 48,000. During the last 12 h before the final fracture of the shaft, a total of 12 start-and-stop operations of the centrifugal pump have been scheduled.

The centrifugal pump was installed and commissioned some 30 years ago. There have been three major repairs of the pump involving leaking of the seal. A mechanical seal was installed on the threaded portion of the shaft with a preload corresponding to 25–30% of the material yield strength. However, no reported abnormality on the shaft was recorded.

A typical operation cycle of the centrifugal pump consists of a start-up and running of the pump at a nominal rotor speed of 2975 rpm for 14 h, with a 2-h complete shut-down interval. The pump operates between 5 and 7 days a week throughout the year.



Figure 2. Failure scenario of the centrifugal pump showing the fractured rotor shaft.

The overall view of the failed centrifugal pump is shown in **Figure 2**. The driving side of the fractured rotor shaft has been removed, while the sleeve remained in place.

4. Visual inspection of the fractured shaft

The simplified geometry of the rotor shaft along with major dimensions is illustrated in **Figure 3**. The drive end of the shaft is connected to the shaft of the motor using the coupler. The distance between the bearing supports is 982 mm. The middle section of the stepped shaft with the largest diameter of 65 mm carries the impeller that is positioned in place with a key. The key way has the dimensions of 9 mm radius, length × width of 60 × 18 mm^2, and the depth of 9 mm. Both ends of this section are threaded with M65 × 1.5 threads to receive the mechanical seals (only the critical threaded portion, located on the right side of the section, is drawn). The shaft fractured at the section through the first thread on the drive side as illustrated in **Figure 3**. The fracture plane is oriented with its normal along the longitudinal axis *(z-axis)* of the shaft.

A closer visual inspection of the fractured surface reveals the morphology as shown in **Figure 4(a)**. A greater portion of the surface was flattened and smeared off due possibly to the repeated grinding against the fracture surface of the mating part while the motor runs after the complete

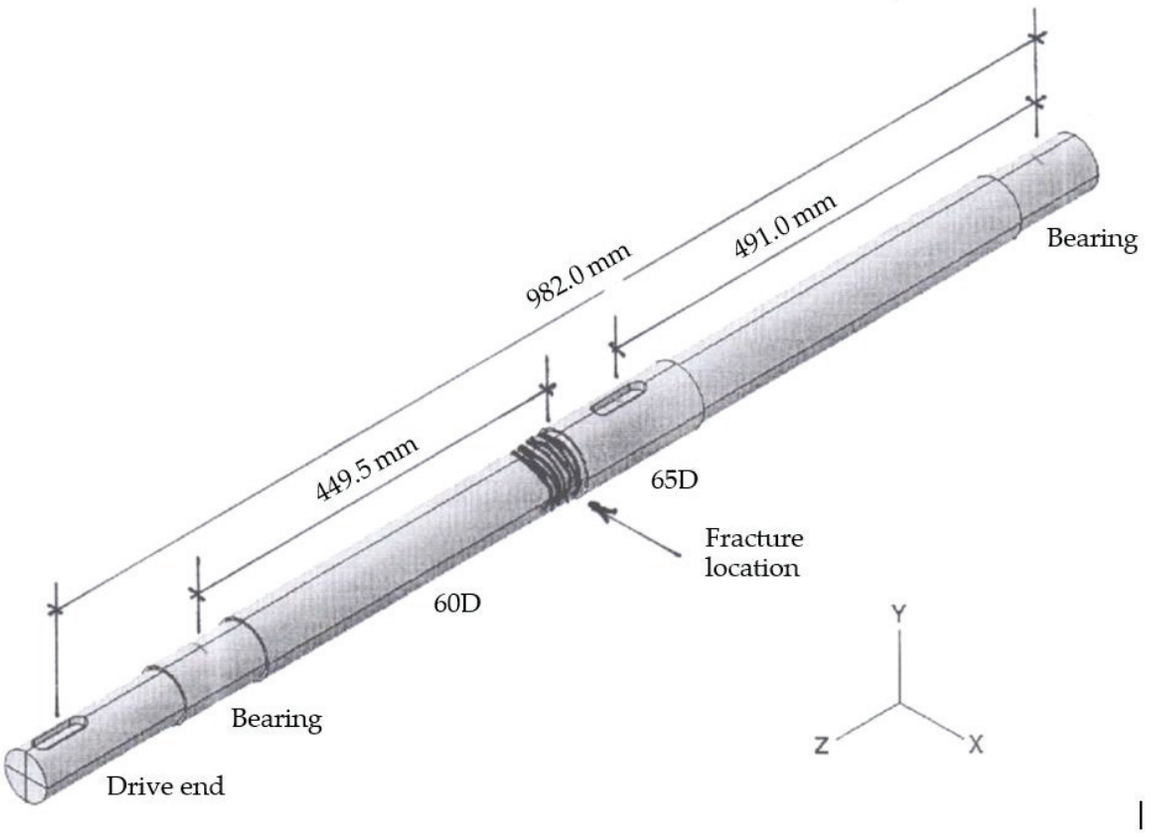


Figure 3. Simplified geometry of the rotor shaft indicating the fracture location.

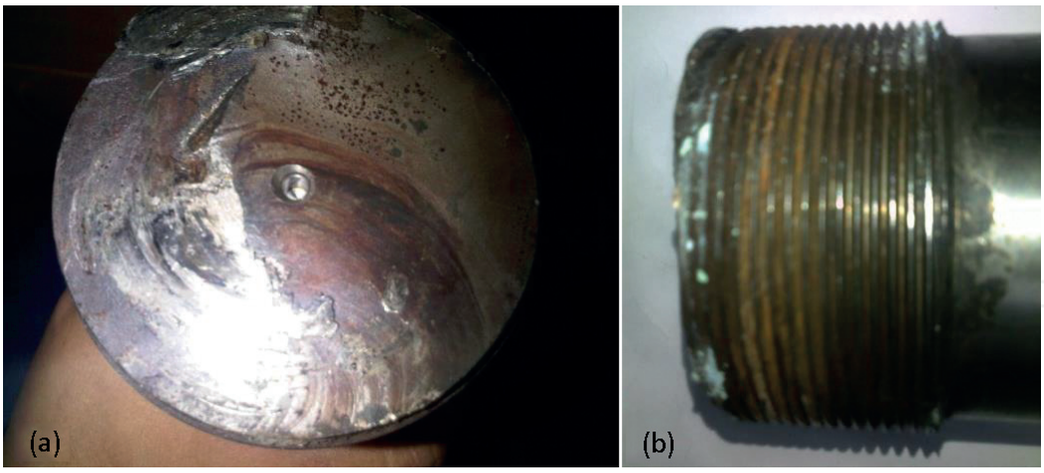


Figure 4. (a) Morphology of the fracture surface, indicating the fatigue *beach lines,* (b) orientation of the fracture plane perpendicular to the longitudinal axis of the shaft.

fracture. Thus, details of the fracture feature could not be extracted easily from the fractograph. However, traces of beach marks indicating fatigue failure are obvious.

It is worth noting that the fracture plane is oriented almost perpendicular to the longitudinal plane of the shaft, as shown in **Figure 4(b)**. Such orientation of the fatigue fracture plane is indicative of the Mode-I (opening) crack propagation under the induced flexural fatigue loading.

5. Chemical design analysis

The chemical design analysis is performed to establish the conformance of the failed shaft material to the manufacturer's materials specification. The manufacturer's record shows that the failed rotor shaft was made of AISI 4140 HT steel. In this respect, the chemical composition of the shaft material is determined using the Glow Discharge Spectrometer (GDS). The resulting chemical composition (in wt. %) is summarized in **Table 3**, the remaining being *Fe*. Other elements detected in the alloy are listed in **Table A1** of the Appendix. The nominal range of the composition for each element of the AISI 4140 steel is also indicated for comparative purposes [1]. It is noted that the failed *Cr-Mo* steel shaft contains slightly higher carbon content, within the range for AISI 4150 steel. Copper is also detected in the failed shaft material.

Microstructures of the steel at two different magnifications are shown in **Figure 5**. The dark and light phases represent tempered and untempered martensite, respectively, with acicular or needlelike structures.

Elem.	***C***	***Mn***	***Cr***	***Mo***	***Si***	***Cu***	***Fe***
Cr-Mo steel shaft	0.502	0.722	1.08	0.228	0.187	0.23	Bal.
AISI 4140	0.38–0.43	0.75–1.00	0.80–1.10	0.15–0.25	0.15–0.30	–	Bal.
AISI 4150	0.48–0.53	0.75–1.00	0.80–1.10	0.15–0.25	0.15–0.30	–	Bal.

Table 3. Elemental composition of the Cr-Mo steel shaft (wt. %) and the reference steel.

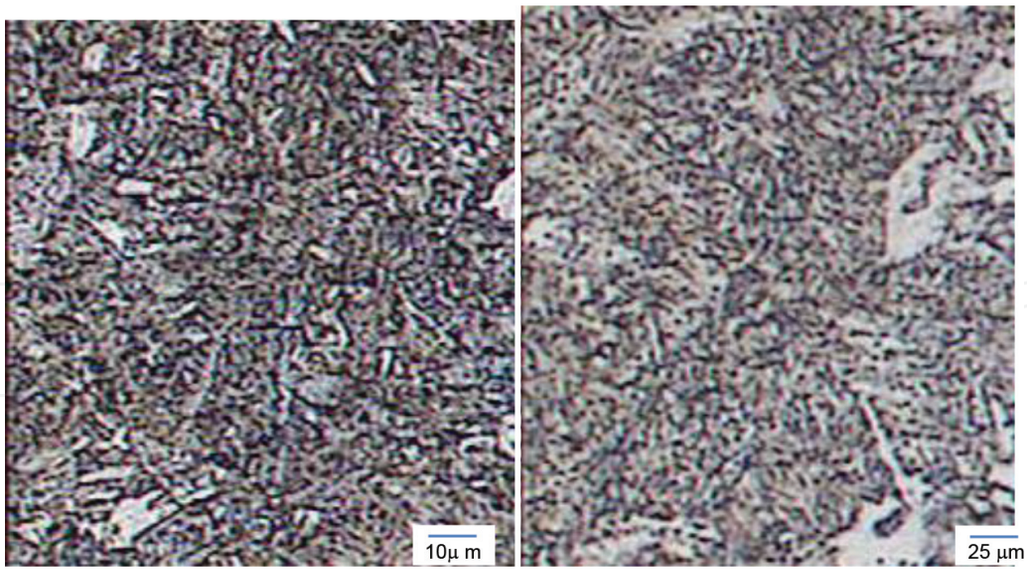


Figure 5. Microstructures of the shaft material showing the matrix of martensite.

Hardness measurements were taken on the failed sample of the steel shaft, at the location near the fractured section. The mean of 20 Vickers hardness readings measured across the section of the shaft is 327.4 HV with a standard deviation of 22.3 HV. The corresponding hardness number on the Brinell and Rockwell C scale is 311 HB and 33 Rc, respectively. Based on the observed microstructures and the hardness measures, it is concluded that the shaft material was likely AISI 4150, oil-quenched, tempered at 595°C. However, the presence of *Cu* could have improved the toughness of the alloy at the expense of lower tensile properties.

6. Mechanical design analysis

Mechanical design analysis is performed to examine the adequacy of the design against yield and fatigue failure of the shaft material. The analyses consist of the stress calculations, particularly at the observed fractured section of the rotor shaft. The critical stress states are then compared to the respective strengths of the shaft material to establish the possible causes of failure. In this respect, the stress levels in the rotor shaft arising from three different load cases are considered, as follows:

i. Stresses during the pumping operation at the rated load. Such stresses could lead to high-cycle fatigue failure of the shaft. The fluctuating load consists of

- a steady torque of T = 834.7 N.m during the power transmission of 260 kW at 2975 rpm from the electric motor to the rotor shaft.
- the cyclic flexural stress induced by the mass of the shaft, assumed to be uniformly distributed along the length of the shaft between the bearing supports (w = 0.12 N/mm). The weight of the impeller generates a concentrated transverse force of 392.4 N.

ii. Stresses during the transient start-and-stop operation: The peak torque at each start-up cycle is up to three times higher in magnitude than that during the nominal operating

speed. Such high torque is derived from the inertia effect of the rotor shaft and the massive impeller.

iii. Additional stresses due to preloading of the lock nut for the mechanical seal: The threaded region where fracture was observed was fitted with a locknut that holds the seal in place. The preload contributes a relatively high mean stress to the existing alternating stress component. In addition, the thread geometry inherits the stress concentration at the root region.

The torsional load sequence experienced by the rotor assembly during a typical loading cycle is illustrated in **Figure 6**. It consists of a short start-up process that exerts three times higher peak torsional load than the nominal load level and a 14-h operation at the rated load. This is followed by a complete shut-down for a 2-h interval. Based on the service record that the rotor assembly was recently balanced, thus the contribution to the failure due to the potentially high dynamic imbalance load is ruled out. The rotor assembly has been in service for 30 years and 3 months at the time of fracture. This corresponds to a total of 16,500 start-and-stop cycles endured by the centrifugal pump system.

6.1. Material properties

The required set of mechanical properties of the *Cr-Mo* steel for use in the stress analysis is obtained from published literature [2, 3]. The properties are based on data for AISI 4140, oil-quenched and tempered at 650°C to 285*HB*. The tensile strength (S_U) and yield strength (S_Y) of the material is 758 and 655 MPa, respectively. The cyclic yield strength $\left(S'_Y\right)$ is estimated at 458 MPa.

The endurance limit (S'_e) is reported to be 420 MPa at 10^7 cycles. Since the reported fatigue limit is often established using smooth specimens, it should be corrected to account for the surface condition at the fracture location and the large diameter of the rotor shaft relative to the fatigue test specimens. The surface of the fractured threaded region was machine-finished, and thus the fatigue limit-modifying factor, k_a = 0.72 (refer to **Figure A1a** of the Appendix). Consider the size effect based on the root diameter of the shaft with M65 × 1.5 threads, the corresponding fatigue limit-modifying factor, k_b = 0.795, as determined from **Figure A1b** of the Appendix.

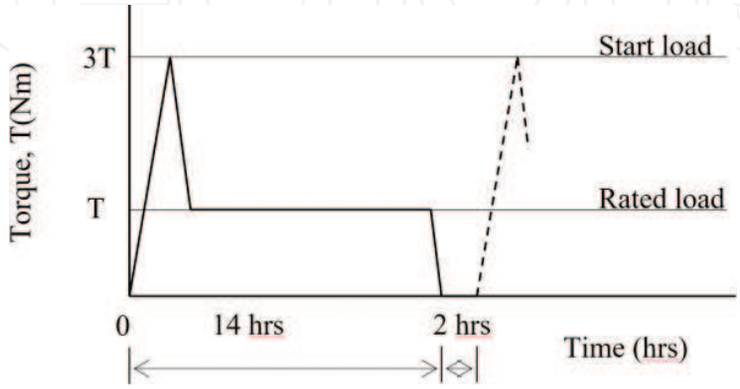


Figure 6. Torsional load sequence experienced by the failed rotor shaft.

The corrected fatigue limit (S_e) is then estimated as

$$S_e = k_a k_b S'_e = (0.72)(0.795)(420) = 240 \text{ MPa} \quad (1)$$

The thread root geometry induces the local stress gradient. Such stress concentration effect is quantified using the fatigue stress concentration factor, K_f. It accounts for the sensitivity of the notched geometry to fatigue stressing. It is defined as the ratio of the endurance limits of notch-free specimens to notched specimens. In this analysis, K_f is treated as a factor that increases the stress, instead of decreasing the fatigue limit of the material. Based on published data for steel-threaded members with hardened and cut threads, the value of K_f is taken as 3.8 (see **Table A2** of the Appendix).

6.2. Fatigue analysis of the shaft at the rated pumping load

Stress analysis is performed for the critical section of the shaft where fracture is observed. Therefore, the calculations are based on the minor diameter of the threaded part for the M65 × 1.5, d = 63.16 mm [4]. The bending moment at the critical section is calculated to be $M_C = 102.5$ kN.mm and the corresponding nominal stress is 4.14 MPa. In a rotating shaft, this stress represents the amplitude of the stress cycles. This stress amplitude is further amplified by the fatigue stress concentration ($K_f = 3.8$) as discussed earlier, to give the operating local stress amplitude, σ_a = 15.75 MPa.

The constant shear stress magnitude of 16.87 MPa is amplified by the geometrical stress concentration associated with the notch root of the thread with K_{ts} = 2.0 (see **Figure A2**). This results in the mean shear stress, τ_m = 33.74 MPa.

Since the magnitude of both the normal stress amplitude, σ_a, and the mean shear stress, τ_m, are small relative to the corrected fatigue limit of the shaft material, S_e, the failure of the rotor shaft due to the rated nominal load is ruled out. In fact, this has been demonstrated by the accumulated fatigue life of the rotor at more than 4×10^{10} cycles during the 30 years of service.

6.3. Fatigue analysis due to start-and-stop operations

Duty cycles of the pump consist of the transient start-and-stop operations, as illustrated in **Figure 6**. The start-up procedure exerts three times higher peak torque ($3T$ = 2504 N.m) to the shaft due to the inertia effect of the rotor assembly. This corresponds to a maximum shear stress of 101.22 MPa. Thus, the transient start-and-stop cycles induce an alternating shear stress, $\tau_{xy,a}$ = 50.61 MPa and a mean shear stress component, $\tau_{xy,m}$ = 50.61 MPa. The bending stress amplitude arising from the dead weight of the shaft and impeller remains at σ_a = 15.75 MPa.

An equivalent fluctuating load, in terms of normal stress components, for the combined loading of fluctuating shear and normal stresses can be defined using the distortion energy theory [5]. The mean, σ'_m, and the amplitude, σ'_a, of the von Mises stress are defined, respectively, as

$$\sigma'_m = \sqrt{\sigma^2_{x,m} + 3\,\tau^2_{xy,m}} = \sqrt{3\,\left(50.61^2\right)} = 87.7\ \text{MPa} \tag{2a}$$

$$\sigma'_a = \sqrt{\sigma^2_{x,a} + 3\,\tau^2_{xy,a}} = \sqrt{\left(15.75^2\right) + 3\,\left(50.61^2\right)} = 89.1\ \text{MPa} \tag{2b}$$

The possibility of fatigue failure due to the transient start-and-stop cycles could then be examined using the modified Goodman failure criterion. Fatigue failure is likely to occur when the criterion value reaches unity:

$$\frac{\sigma'_a}{S_e} + \frac{\sigma'_m}{S_U} = \frac{89.1}{240} + \frac{87.7}{758} = 0.49 \tag{3}$$

The operating localized stress condition due to the start-and-stop cycles is shown as Point *A* on the fatigue diagram, as illustrated in **Figure 7**.

Since the value of the modified Goodman criterion reaches only 0.49, the accumulated start-and-stop cycle is unlikely to cause the observed fatigue failure. In addition, the rotor assembly has only completed about 16,500 start-and-stop cycles prior to the fracture event.

It is then postulated that the localized stresses at the fractured section must have been higher than that previously calculated. This could have been contributed by the tightening of the mechanical seal unit. Such preloading of the sleeve for the mechanical seal induces a mean normal stress component in addition to the existing alternating stress at the critical thread root location. This postulate is examined in the next section.

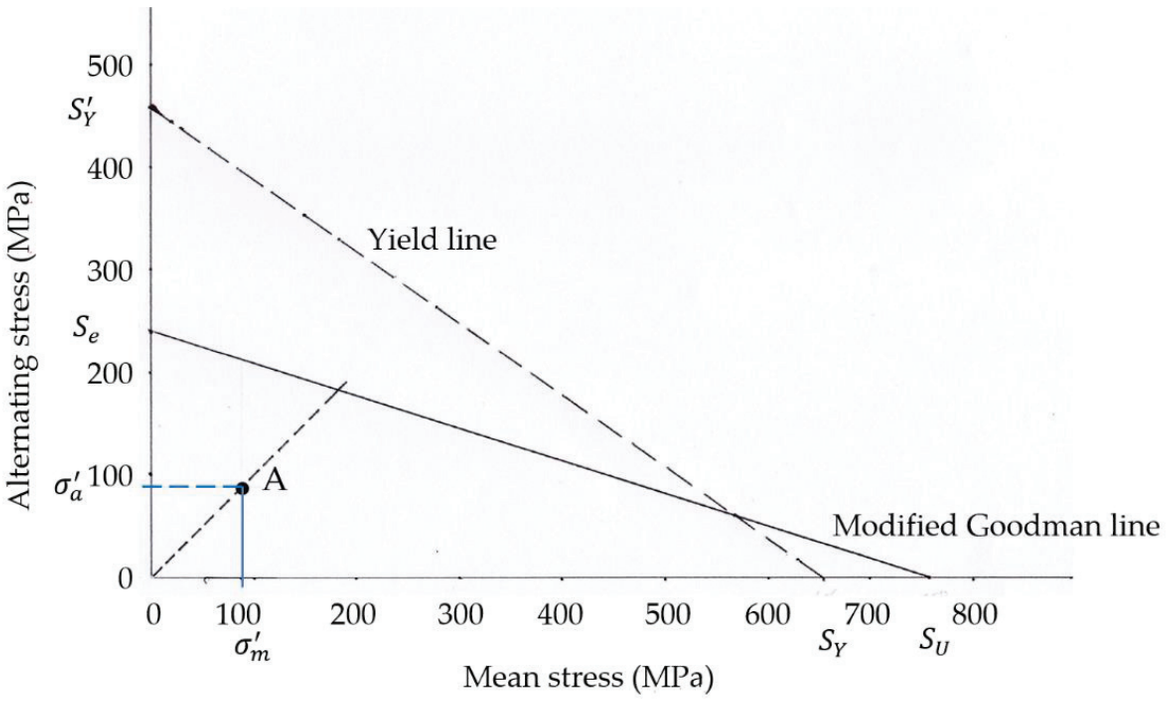


Figure 7. Fatigue life diagram illustrating the modified Goodman failure line and the operating stress condition.

6.4. Contribution of the preload to the local stresses in the threaded region

The tensile force resisted by the threaded shaft, $F_{b,}$ from the tightening of the sleeve for the mechanical seal can be expressed as the sum of initial tightening force, $F_{i,}$ and the portion of the externally applied force (bending), $F_{\text{ext},}$ as [6]

$$F_b = F_i + \frac{k_b}{k_b + k_c} F_{ext} \tag{4}$$

The term $\frac{k_b}{k_b+k_c}$ represents the effective stiffness of the threaded shaft and the clamped sleeve of the mechanical seal. The effective stiffness term is proportional to the "effective" shaft section and the clamped area, $C = \frac{A_b}{A_b+A_c}$. The external force represents the induced bending by the dead weight of the rotor assembly. The resisting normal stress in the threaded shaft, $\sigma_b = \frac{F_b}{A_t}$, can then be expressed as

$$\sigma_b = K_t \sigma_i + \frac{A_b}{A_b + A_c} \sigma_{bending} \tag{5}$$

This stress contributes to the mean normal stress component at the critical root region of the threaded shaft. Taking the geometrical stress concentration factor for the cut thread, K_t = 3.0, and estimating the effective threaded shaft section, C = 0.33, the mean stress, $\sigma_{x\,,\,m}$, is

$$\sigma_{x,m} = \sigma_b = (3.0)\sigma_i + (0.33)(15.75) \tag{6}$$

The sensitivity of the initial tightening force ($F_i = \sigma_i A_t$) on the resulting fatigue life is examined using Eqs. (2a), (2b), (3), and (6). The allowable initial force is the magnitude to induce the stress up to the proof strength of the shaft material, $S_p = 0.9S_Y = 589.5$ MPa. The simulated result indicates that an initial preload of the threaded joint to $0.25S_Y$ would have resulted in an equivalent von Mises fluctuating stresses with $\sigma'_m = 499.1$ MPa, while the alternating component remains at $\sigma'_a = 89.1$ MPa. This stress condition is indicated by Point B as shown in **Figure 8**. The corresponding modified Goodman criterion value of 1.03 suggests a fatigue failure condition at 10^7 start-and-stop cycles. However, we recall that the accumulated start-and-stop cycles at failure are about 16,500 cycles.

The fatigue strength of the shaft material corresponding to the observed finite life of N_f = 16,500 cycles is estimated based on the Basquin equation to be S_{Nf} = 499 MPa. Since this fatigue strength is greater than the cyclic yield stress of the material, the observed failure is likely governed by localized plasticity. This stress condition is represented by Point C in **Figure 8**.

It is concluded that fatigue crack nucleated in the localized plastic zone at the threaded root region of the shaft. The relatively high mean stress component is induced by the preloading of the threaded sleeve. Under continuous fatigue loading, the crack traverses the shaft cross section leading to premature fatigue failure of the rotor shaft.

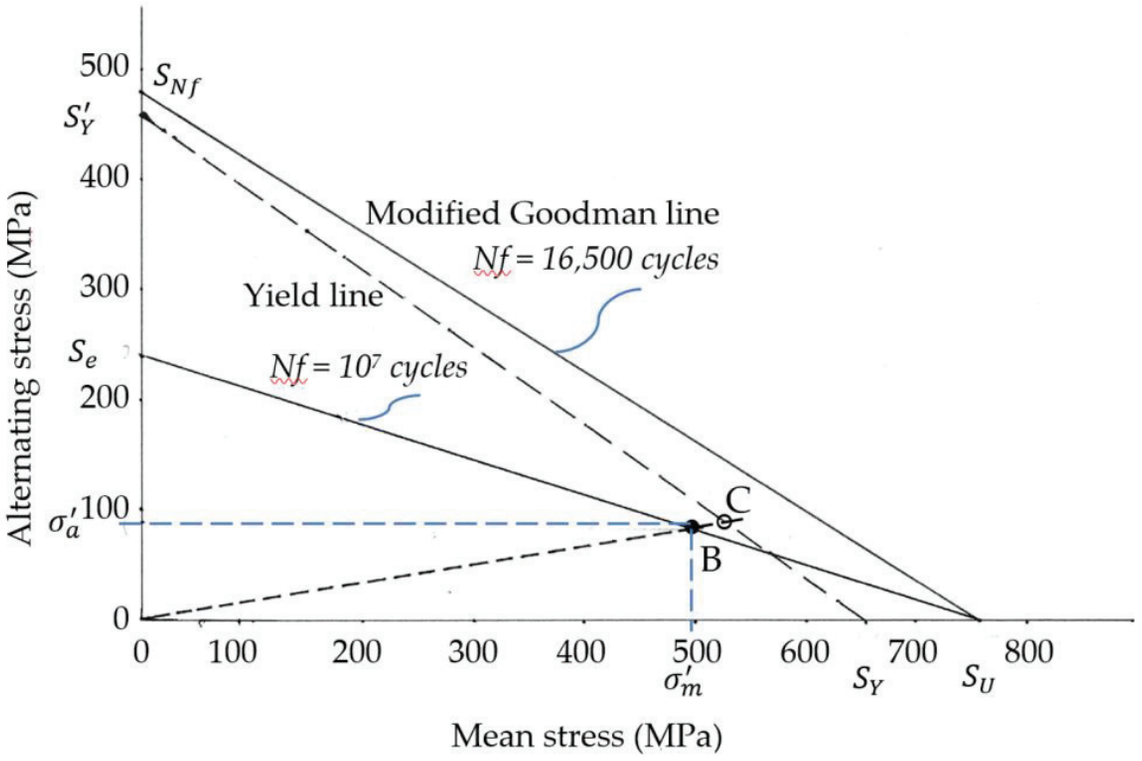


Figure 8. Fatigue life diagram illustrating the possible stress conditions with preload at $0.25S_Y$; fatigue failure (Point B) and yield (Point C).

7. Concluding remarks

Numerous machine components, including the rotor shaft of a centrifugal pump, are load-bearing structures. Since the shaft experiences fluctuating load, fatigue is a common source of the failure. Evidence of fatigue failure is often traceable to the visible beach lines on the fractured surface. However, the cause of failure must be demonstrated through the mechanics-of-deformation analysis involving stress calculations. Unfortunately, the much-needed set of mechanical properties of the material for accurate analysis is often unavailable, thus intelligent estimation is inevitable.

The classical fatigue analysis, as demonstrated in this chapter, is based on constant-amplitude loading. The effect of the transient start-and-stop cycles on the resulting fatigue life of the rotor shaft is not easily accounted for. However, in each analysis involving the rated load cycles and the start-and-stop cycles, premature high-cycle fatigue is an unlikely cause of the failure.

The inherent continuous fatigue degradation of the strength properties is not considered in the strength-of-materials analysis, often performed for failure investigation. However, this classical mechanics analysis is adequate, in most cases, in establishing the cause of failure. The more accurate, yet involved failure prediction based on damage mechanics approach is beyond the scope of this chapter.

Appendices

See **Tables A1**, **A2** and **Figures A1** and **A2**.

	FE (%)	C (%)	Mn (%)	P (%)	S (%)	Si (%)	Cu2 (%)	Ni2 (%)	Cr2 (%)	V (%)	Mo (%)	Ti (%)
Burn 1	96.8	0.509	0.72	0.0137	0.0247	0.188	0.288	0.0619	1.08	0.0079	0.225	0.0116
Burn 2	96.9	0.501	0.723	0.0135	0.0247	0.187	0.205	0.0614	1.08	0.00777	0.226	0.011
Burn 3	96.9	0.497	0.722	0.0134	0.0247	0.186	0.197	0.0614	1.08	0.00758	0.226	0.0109
AVG	96.8	0.502	0.722	0.0135	0.0247	0.187	0.23	0.0616	1.08	0.00775	0.226	0.0112

	Al (%)	Nb (%)	Zr (%)	B2 (%)	B (%)	Sb (%)	Co (%)	Sn (%)	Sn2 (%)	Pb (%)
Burn 1	0.0298	0.00326	0.0112	0.000769	0.000787	0.00696	0.0183	0.0149	0.0115	0.00503
Burn 2	0.03	0.00233	0.0104	0.000723	0.000704	0.00529	0.0182	0.0133	0.0105	0.00418
Burn 3	0.0301	0.00163	0.0097	0.000691	0.000729	0.0053	0.0175	0.0118	0.00949	0.00424
AVG	0.03	0.00241	0.0104	0.000728	0.00074	0.00585	0.018	0.0133	0.0105	0.00449

Table A1. Chemical composition of Cr-Mo steel by GDS analysis.

Hardness	SAE grade (unified thds.)	SAE class (ISO thds.)	K_f rolled thds.	K_f cut thds.
Below 200 Bhn (annealed)	2 and below	5.8 and below	2.2	2.8
Above 200 Bhn (hardened)	4 and above	8.8 and above	3.0	3.8

Table A2. Fatigue stress concentration factors for steel-threaded members [6].

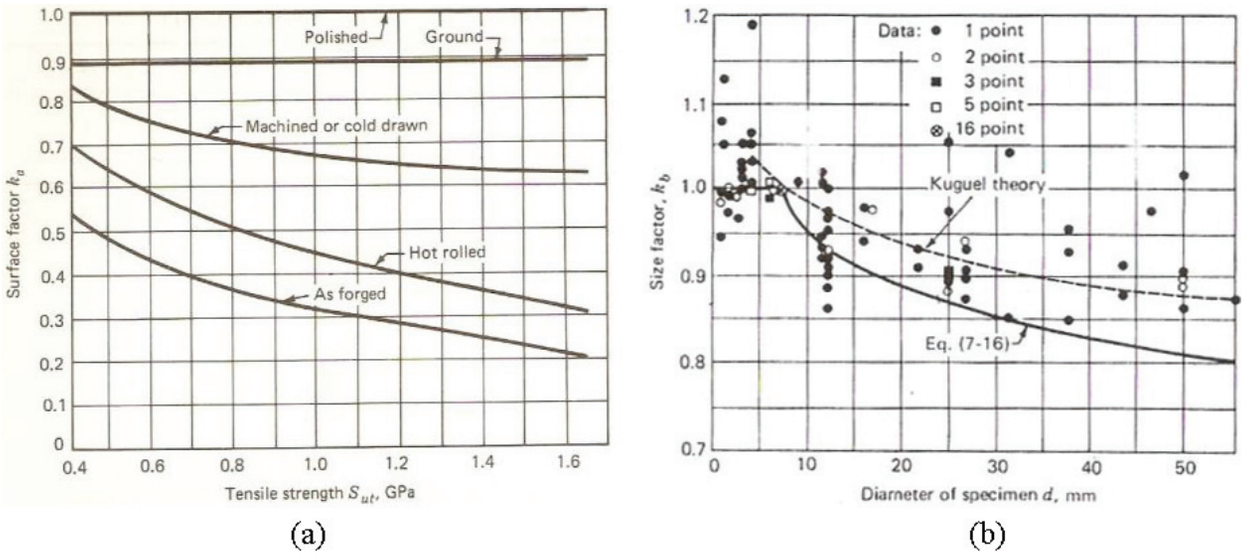


Figure A1. Endurance limit-modifying factors used for the steel shaft [5]. (a) Surface-finish modification factors, (b)Effect of specimen size on the endurance limit in reversed bending and torsion.

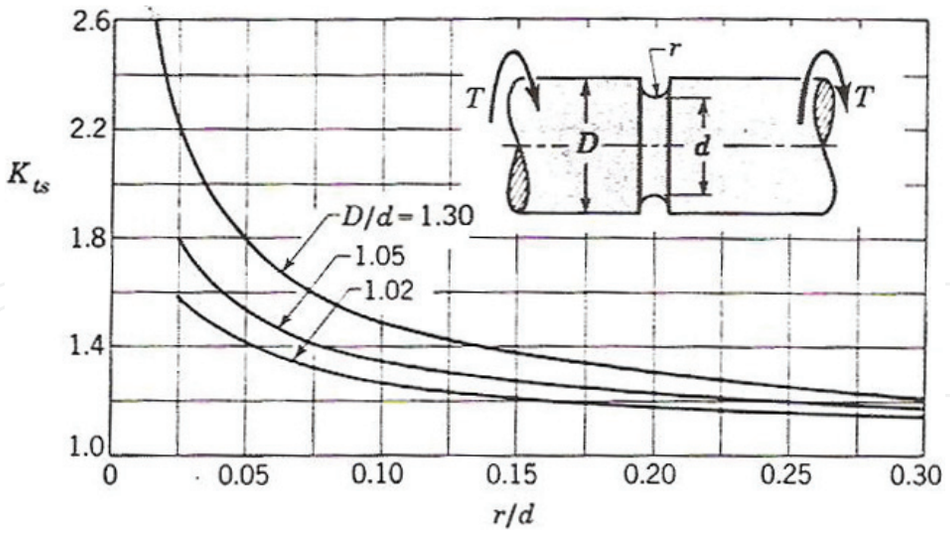


Figure A2. Geometric stress concentration factor chart [5].

Author details

Mohd Nasir Tamin[1]* and Mohammad Arif Hamzah[2]

*Address all correspondence to: nasirtamin@utm.my

1 Faculty of Mechanical Engineering, Universiti Teknologi Malaysia, Johor Bahru, Johor, Malaysia

2 Sarawak Shell Malaysia Berhad, Kuala Lumpur, Malaysia

References

[1] Avner SH. Introduction to Physical Metallurgy. 2nd ed. New York, USA: McGraw-Hill; 1974

[2] Mechanical Properties of 4140 Steel. July 2017. Available from: https://icme.hpc.msstate.edu/mediawiki/index.php/Mechanical_properties_of_4140_steel

[3] Stephen RI et al. Metal Fatigue in Engineering. 2nd ed. New York, USA: Wiley Interscience Publication; 2000

[4] Maryland Metrics Thread Data Charts, Metric Thread-Coarse Pitch-M. July 2017. Available from: https://mdmetric.com/tech/thddat2.htm

[5] Shigley JE. Mechanical Engineering Design. Singapore: McGraw-Hill; 1986

[6] Juvinal RC. Fundamentals of Machine Component Design. New York, USA: John Wiley & Sons; 1983